From molecular Sb units to infinite chains, layers, and networks: Sb–Sb interactions in metal-rich antimonides

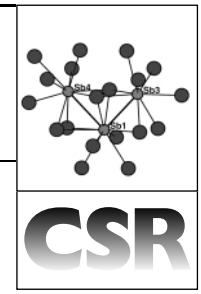

Holger Kleinke

Department of Chemistry, University of Waterloo, Waterloo, Ontario, Canada N2L 3G1

Received 6th March 2000
First published as an Advance Article on the web 4th October 2000

A multitude of metal-rich pnictides and chalcogenides of the valence-electron-poor transition elements *M* have been uncovered in recent years. Common structural features of all these compounds are extended metal atom substructures (of different kinds) and the occurrence of metal–pnicogen and metal–chalcogen bonds, respectively. Bonding homonuclear interactions between the main-group elements *E* are found only in the structures of the antimonides and bismuthides. This bonding situation is associated with highly complex crystal structures in the latter cases, because of the presence of three different types of bonding, *i.e. M–E*, *M–M* and *E–E* bonds.

1 Introduction

In the nineties, there was a strongly renewed interest in the investigation of metal-rich pnictides and chalcogenides of the valence-electron-poor transition elements *M*, as the number of recent publications show. An electron transfer occurs in principle from the *M* atoms to the more electronegative main-group elements *E*, which results often—but not always—in a complete reduction of the *E* atoms. Throughout this article, the term *metal rich* is used for compounds whose *M*:*E* ratio is— in theory—high enough to give completely reduced *E* atoms, while some valence-electrons of *M* remain available for the formation of *M–M* bonds. However, this does not imply that all *E* atoms are completely reduced in metal-rich compounds; in contrast, the opposite case is the main topic of this review.

The definition excludes electron-precise compounds such as $M^{3+}Sb^{3-}$ with *M* = Sc, Y, La (*M*:*E* = 1),[1] but includes compounds with smaller *M*:*E* ratios like Ta_2Te_3.[2] The latter can be understood based on the ionic formulation $(Ta^{3+})_2(Te^{2-})_3$, with the two electrons remaining per Ta atom taking part in Ta–Ta bonding.

Most of the recent examples of metal-rich pnictides and chalcogenides have new types of structures, including Sc_2Te,[3] $(Zr,V)_{13}Sb_{10}$,[4] $(Zr,Nb)_{11}P_4$,[5] Hf_3Te_2,[6] $(Nb,Ta)_5S_2$,[7] Ta_2Te_3,[2] Ta_6Te_5 and dd-$Ta_{1.6}Te$.[8] These compounds exhibit significant differences in their crystal structures, which range from three-dimensional structures through layered to chain compounds, as well as in their physical properties (metallic/non-metallic). Five different classes of compounds, based on their different metal atom substructures, have been discussed recently for the phosphides and sulfides.[9]

Most of the compounds discussed here belong to one of the three following groups. The first group, which is the most common, comprises compounds in which the metal atoms form (distorted) fragments of body-centered cubes [*e.g.* Sc_2Te, $(Zr,Nb)_{11}P_4$, Hf_3Te_2, $(Nb,Ta)_5S_2$]. The second group comprises compounds having a metal atom substructure related to hexagonal close packing (*e.g.* Hf_2S[1]). The third group is dominated by the members with tantalum as the transition element. Therein, the *M* atoms build *M*-centered icosahedral units (*e.g.* in the quasicrystalline telluride dd-$Ta_{1.6}Te$, or in Ta_6S[1]). In all three groups, the *E* elements are located in somewhat capped trigonal prisms formed by the *M* atoms or fragments thereof. It is remarkable that no antimonides are known to belong to any of these three groups. Mention should also be made of some other exceptional structures, which are related to typical intermetallics, namely the κ-phases ($Hf_9Mo_4SO_x$ and $Hf_9W_4SO_x$) or the filled γ-brass $(Hf,Ta)_{13}S_3$.[10]

Since in the pnictides and chalcogenides of the valence-electron-poor transition metals with *M*:*E* ratios > 3/4, bonding homoatomic *E–E* interactions occur only in the cases of the antimonides and bismuthides, they stand out in this family. To date, very little is known about the bismuthides. One very recently published metal-rich silicide phosphide, $Hf_{27}(Si,P)_{16}$, also exhibits some bonding interactions between the main group elements *E* within an E_2 pair. However, due to the possibility of Si/P mixing on all *E* sites, one could assume 100% Si occupancies on the sites participating in the E_2 pairs, and thus purely Si–Si bonding.[11]

This bonding situation in the antimonide results in highly complex crystal structures, compared to those of the other pnictides and chalcogenides, because of the presence of three different types of bonding, *i.e. M–E*, *M–M* and *E–E* interactions. It might appear at first paradoxical to have homonuclear bonds between the cationic as well as the anionic constituent elements of any compound, *i.e.* polycationic units together with polyanionic motifs within one single compound, but in general this is possible for phases consisting of elements with rather small differences in electronegativity. An overview of the earliest pnictides and chalcogenides was given in 1968.[12]

Holger Kleinke, born in 1966, studied chemistry at the Westfälische Wilhelm-Universität Münster in Germany. He received his PhD in 1994 under the guidance of Wolfgang Tremel at the Johannes-Gutenberg Universität Mainz, Germany. He was a DFG postdoctoral fellow in Hugo F. Franzen's group at the Ames Laboratory, Department of Energy, in Iowa, USA (1995–1997). Thereafter, he started to work on his 'Habilitation' in 1997 in the group of Bernd Harbrecht in Marburg, Germany, as a Liebig fellow (FCI), followed by a DFG 'Habilitandenstipendium' (1999). In 2000, he joined the Department of Chemistry at the University of Waterloo in Ontario, Canada.

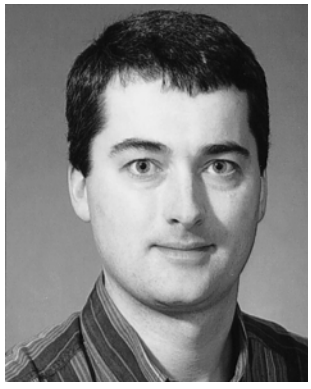

2 Classification of Sb–Sb bonds

The structure of antimony, being isostructural with gray arsenic, consists of puckered layers with interatomic distances of 291 pm, which are interconnected *via* longer distances of 335 pm. The truly three-dimensional properties reveal bonding character of the latter interactions as well, which is supported by the small but positive Mulliken overlap population (*MOP*) of 0.08,[13] and by the band broadening arising from the overlap,[14] as obtained by Extended Hückel calculations.[15] Weak bonding interactions were also detected for even longer distances: *ab initio* calculations at the second-order Møller-Plesset level (MP2) indicated a Sb–Sb attraction due to correlation effects in the hypothetical diantimony hydride model dimer $(H_2Sb–SbH_2)_2$ with a Sb–Sb distance of 378.5 pm, supported experimentally by measurements of the force constant in $Sb_2(CH_3)_4$ ($d_{Sb–Sb}$ = 368 pm).[16] The long intermolecular bond exhibits a force constant of more than 10% of the one of the short intramolecular single bond ($d_{Sb–Sb}$ = 284 pm).

One cannot, therefore, neglect any Sb–Sb distances < 350 pm. *MOP*s can serve as relative values for bond strengths, and reference values are: typical Sb–Sb single bonds (*e.g.* in KSb: $d_{Sb–Sb}$: 283–285 pm, *MOP*: 0.66–0.63) and the shortest bond in the element (*MOP* = 0.53).[13] A very similar approach to scale Sb–Sb bonds based on the *MOP*s was used in a discussion of the electronic structure of $La_{12}Mn_2Sb_{30}$.[17]

3 Molecular Sb units in metal-rich antimonides

Only in the most metal-rich examples are antimonides isostructural to the tellurides, although Sb and Te atoms are comparable in size and—to a smaller extent—in electronegativity. For example, Zr_3Sb[1] and Zr_3Te[18] both occur in the Ni_3P structural type without any *E*–*E* distances < 400 pm, where the *E* atoms are located in a three-capped trigonal prism, *i.e.* a deltahedral tetrakaidecahedron. The dimetal monoantimonides M_2Sb and pentametal tris-antimonides M_5Sb_3 occur in structural types typical of antimonides, namely Sc_2Sb (Cu_2Sb type), La_2Sb and Zr_2Sb (La_2Sb), Zr_5Sb_3[1] and Hf_5Sb_3 (Y_5Bi_3).[19] Therein, the Sb atoms are surrounded solely by eight to nine *M* atoms. While the antimonides M_2Sb do fit into a structure map recently introduced for metal-rich pnictides and chalcogenides M_2E, they occur in the outermost right part of it, thus playing a special role.[20]

The most metal-rich antimonide of the valence-electron-poor transition elements with Sb–Sb distances < 350 pm is $(Hf,Ti)_7Sb_4$. This compound can be prepared by arc-melting under an inert gas atmosphere (*e.g.* argon), being stable with respect to disproportionation upon annealing at 1000 °C. Its unprecedented structure was solved for $Hf_{7-x}Ti_xSb_4$ with x = 1.05(7), with all *M* sites being mixed occupied in different Hf : Ti ratios between 8 : 1 and 4 : 1.[21] Since this structure cannot be obtained in either of the binary systems Hf–Sb and Ti–Sb, the differential fractional site occupancies significantly enhance its stability. Therefore, $(Hf,Ti)_7Sb_4$ is classified as a typical DFSO material.[22]

In a mnemonically useful approach, the structure can be described based on metal atom sheets forming 488 nets (Fig. 1), which are interconnected *via* *M*–*M* and *M*–Sb bonds and common Sb atoms to a truly three-dimensional structure. The two distinct 488 nets differ in the deviations from the ideal squares and octagons as well as in their surroundings, the sheet not shown in Fig. 1 occurring as a double layer.

The structure of $(Hf,Ti)_7Sb_4$ exhibits two different Sb units, namely a nonlinear Sb_3 unit and one Sb atom (Sb2) without any neighboring Sb atom being closer than 372 pm (Fig. 2). The shortest Sb–Sb distances in these units are $d_{Sb1–Sb3}$ = 328, $d_{Sb1–Sb4}$ = 344, and $d_{Sb2–Sb2}$ = 372 pm. The Sb2, Sb3, and Sb4

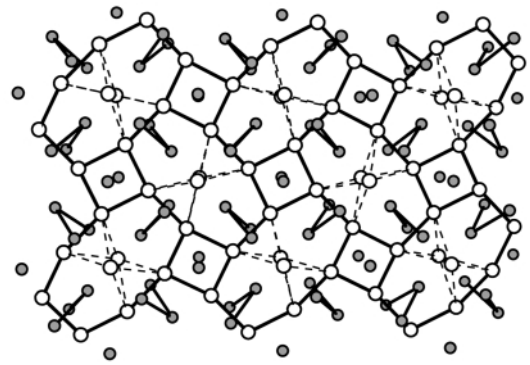

Fig. 1 *M* layer **A** of the structure of $(Hf,Ti)_7Sb_4$, including Sb1 atoms, sheathed by M1 and Sb2,3,4 atoms. White circles: Hf/Ti; gray: Sb. Thick lines emphasize the 488 tiling and the Sb_3 units, respectively.

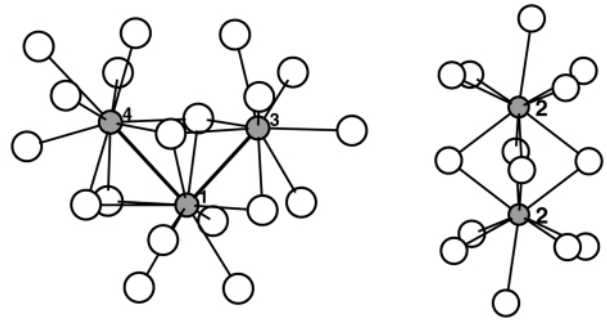

Fig. 2 First coordination spheres of the Sb atoms of $(Hf,Ti)_7Sb_4$.

atoms all are shifted out of the centers of the (severely distorted) surrounding Hf_8 square antiprisms: while the shift of the Sb2 atoms increases the Sb2–Sb2 distance, the Sb3 and Sb4 atoms are moved out of the centers both towards the Sb1 atom. These observations suggest antibonding Sb2–Sb2, but bonding Sb1–Sb3 as well as bonding Sb1–Sb4 interactions.

The electronic structure of $(Hf,Ti)_7Sb_4$ was calculated with the Extended Hückel approximation using the hypothetical structure model Hf_7Sb_4, *i.e.* the structure parameters were taken from the structure refinements on $Hf_{5.95}Ti_{1.05}Sb_4$ with Hf parameters used for all *M* sites. The densities of states (DOS, left part of Fig. 3) at the Fermi level E_F are dominated by the 5d

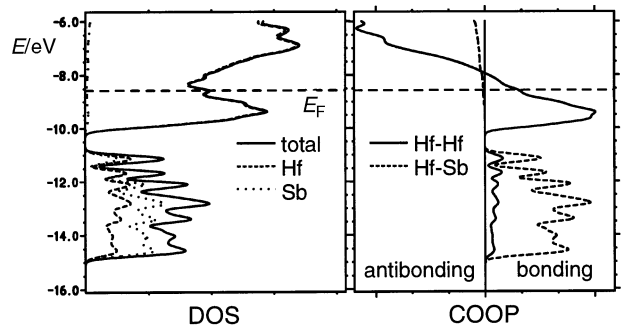

Fig. 3 Densities of states (DOS, left) and selected crystal orbital overlap populations (COOP, right) of the structure model Hf_7Sb_4. Dashed horizontal line: Fermi level E_F.

states of hafnium, while the 5p states of antimony predominate the peak between −6.5 and −2 eV below E_F. That a small tail of the latter goes up above E_F indicates the presence of partly empty Sb orbitals, leading to the ionic formulation $(Hf^{+1.71-4/7\delta})_7(Sb^{-(3-\delta)})_4$ with a small δ. Then, roughly 2.3 electrons per Hf atom are available for the formation of Hf–Hf bonding. However, since the covalency of the Hf–Sb bonds is revealed by the mixing of the Hf states with the Sb *p* states, one should not push this formulation too far. Still, it readily explains

the occurrence of strong Hf–Sb and Hf–Hf bonding, as shown with the corresponding crystal orbital overlap populations (COOP curves) in the right part of Fig. 3.

The COOP curves of the two Sb–Sb interactions within the Sb_3 unit (Fig. 4) reveal three facts in both cases. First, there is

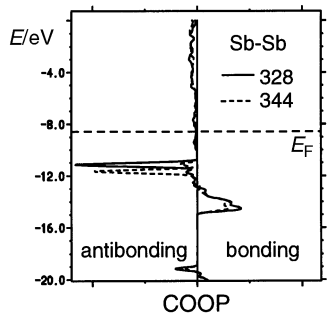

Fig. 4 Selected Sb–Sb COOP curves of Hf_7Sb_4.

significant overlap; second, a lot of antibonding states are filled; third, some antibonding states remain empty. The first observation is a consequence of the short distances, the second is due to the high degree of filled s and p states, and the third shows that at least some p orbitals are not completely filled. It is concluded that the oxidation states of Sb atoms participating in the Sb_3 unit are close to but below −III. On the other hand, nothing suggests the oxidation state of Sb2 being any less than −III. The assumption, that Sb2 is more reduced than Sb1, Sb3 and Sb4, is supported by the Mulliken charges, which range from −0.32 to −0.35 for the latter, compared to −0.42 for Sb2. Integrating over all filled bonding and antibonding states results in small but positive Mulliken overlap populations of 0.05 for the shorter and 0.02 for the longer bond. These *MOP* values are of the order, but somewhat smaller, of that of the longer bond in elemental antimony (d = 335 pm; *MOP* = 0.08), indicating comparable bond strengths.

To summarize, the structure of $(Hf,Ti)_7Sb_4$ is stabilized by strong Hf–Sb and Hf–Hf interactions and, to a minor extent, by Sb–Sb interactions also. The latter is in contrast to the bonding situations in the antimonides Hf_5Sb_3 and Ti_5Sb_3 with comparable M:Sb ratios of 1.6 ($(Hf,Ti)_7Sb_4$: 1.75), whose structures both exhibit only *M*–Sb and *M*–*M* bonding.

4 Infinite Sb chains in metal-rich antimonides

Within the past two years, a novel family of metal-rich antimonides has been discovered, whose crystal structures contain linear chains as well as zigzag chains formed by Sb atoms. The smaller M:Sb ratios between 1.375 and 1, compared to 1.75 in $(Hf,Ti)_7Sb_4$, come along with higher extensions of the Sb atom substructures and shorter Sb–Sb separations as well. So far, four members have been published, namely $(Zr,V)_{13}Sb_{10}$ (new type structure),[4] $(Zr,V)_{11}Sb_8$[23] and $Ti_{11}Sb_8$[24] (both $Cr_{11}Ge_8$ type), and (Zr,Ti)Sb (new type).[25] The structures of the ternaries exhibit as common features:

i) *M* sites at least in part mixed occupied by the 3d (*i.e.*, Ti or V) and 4d (Zr) metal atoms,

ii) metal atom channels (M^1) mainly formed by the 4d atoms, which surround linear Sb chains with $280 < d_{Sb–Sb} < 290$ pm, and

iii) extended NiAs type fragments including zigzag Sb chains with $329 < d_{Sb–Sb} < 350$ pm, whose *M* sites (M^2) are clearly dominated by the 3d metal atoms. (Obviously, the structure of $Ti_{11}Sb_8$ contains only one kind of metal atoms, namely Ti.)

Since the structures of all three ternaries are unknown in all of the corresponding binary systems, one can classify these antimonides like $(Hf,Ti)_7Sb_4$ as DFSO-stabilized materials also. A projection of the structure of $(Zr,V)_{13}Sb_{10}$ along the shortest axis is shown in Fig. 5, emphasizing the two main structure motifs. Both motifs are interconnected *via* a multitude of *M*–*M* and *M*–Sb bonds, which are omitted in the figure for the sake of clarity.

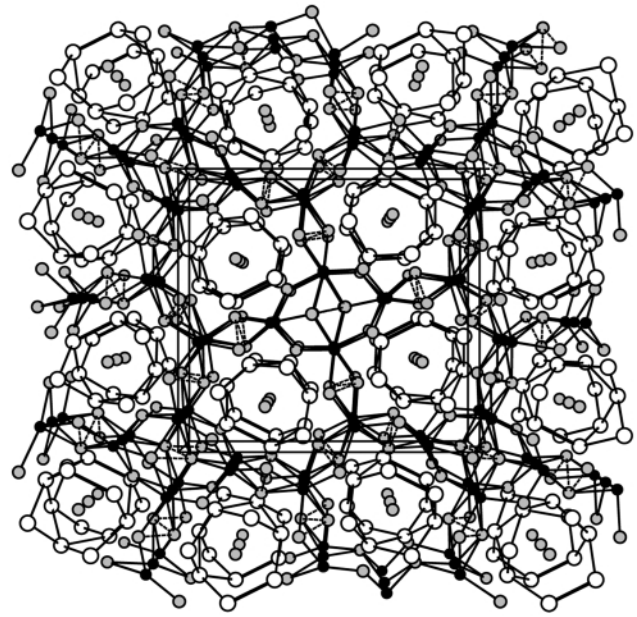

Fig. 5 Projection of the structure of $(Zr,V)_{13}Sb_{10}$ along [010]. Horizontal: *a* axis. White circles: M^1; black: M^2; gray: Sb.

In the projection of $(Zr,V)_{13}Sb_{10}$, the M^1 channels form a semi-regular quadratic-triangular 3^2434 tiling, embedded between the NiAs type fragments. No direct contacts connect the M^1 channels, while they form double chains interconnected by M^1–M^1 bonds in the case of the more metal-rich antimonide $(Zr,V)_{11}Sb_8$ (left part of Fig. 6). Therein, the secondary tiling of these channels is based on a triangular 3^6 net, *i.e.* the channels are stacked like densely packed rods.

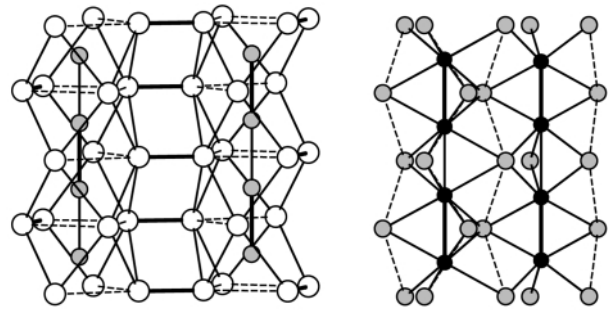

Fig. 6 Columnar structure motifs of $Zr_{7.5}V_{3.5}Sb_8$. Left: part of the $_\infty{}^1[M^1{}_7Sb_2]_2$ chain; right: part of the NiAs-like fragment.

Chains of face-condensed M^2Sb_6 octahedra (or $M^2Sb_5\square_1$ fragments thereof, with □ = vacancy) run parallel to M^1 channels in both cases. As a consequence, the averaged interatomic distances within the linear M^2 and Sb chains are the same, namely $b/2 \approx 285$ pm. Since this is shorter than the strong bond in elemental antimony with d = 291 pm, strong bonding character is assumed. Furthermore, a view at the columnar structure motifs reveals that the Sb atoms of the NiAs-like type fragments form zigzag chains with interatomic separations of 341–344 pm in the structure of $(Zr,V)_{11}Sb_8$ (dashed lines in the right part of Fig. 6). Comparable distances occur in $(Zr,V)_{13}Sb_{10}$ (334–349 pm), which resemble the longer bond in the element antimony (335 pm).

The most striking difference between the two zirconium vanadium antimonides on one hand and the zirconium titanium antimonide on the other is found in the M^1 channels, which

include two linear Sb chains with interatomic distances d = 284 pm in the case of (Zr,Ti)Sb, interconnected *via* longer Sb–Sb contacts of *ca*. 347 pm. This results in a ladder-like arrangement of the Sb atoms in (Zr,Ti)Sb. Furthermore, the NiAs type units are extended only in two dimensions, namely in the *b*,*c* plane. They are separated along the *a* axis by Sb atoms and the M^1 channels. While here two of these layers occur within one unit cell, being related to another by an inversion center and thus staggered with respect to each other (Fig. 7), layers topologically equivalent by translational symmetry were found in the structure of $LnM'Sb_3$, which also comprises planar Sb layers (with Ln = La, Ce, Pr, Nd, Sm, Tb, Dy; M' = V, Cr).[26]

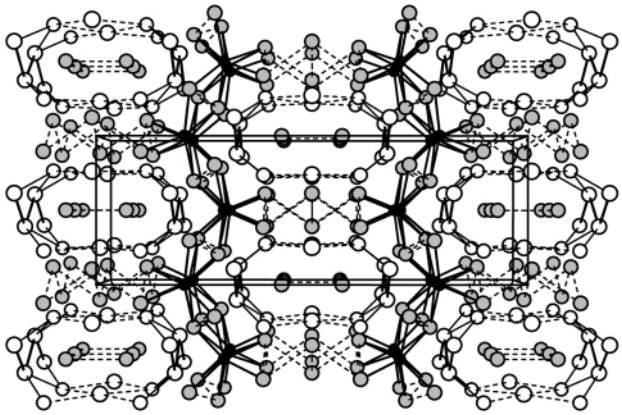

Fig. 7 Projection of the structure of (Zr,Ti)Sb along [001]. Horizontal: *a* axis. White circles: M^1; black: M^2; gray: Sb.

In the structures of $(Zr,V)_{13}Sb_{10}$ and $(Zr,V)_{11}Sb_8$, the Sb atoms of the linear chains are surrounded by $M^1{}_7\square_1$ square antiprisms, while the linear Sb chains of (Zr,Ti)Sb are located in chains of face-condensed $M^1{}_6$ octahedra, which are interconnected *via* common edges to form double chains (Fig. 8).

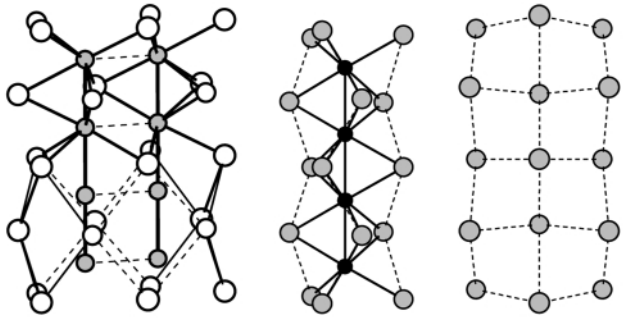

Fig. 8 Columnar structure motifs of (Zr,Ti)Sb. Left: part of the $_\infty{}^1[M_{10}Sb_4]$ chain; middle: part of the NiAs-like fragment; right: section of a 4^4 net of Sb atoms.

Sections of puckered 4^4 nets of Sb atoms, which have no counterpart in the vanadium containing antimonides, run parallel to these chains, as do the NiAs type chains of M^2Sb_6 octahedra.

As postulated based on the crystal structures, *i.e.* on the three-dimensional extended metal atom substructures, all four phases $(Zr,V)_{13}Sb_{10}$, $(Zr,V)_{11}Sb_8$, $Ti_{11}Sb_8$, and (Zr,Ti)Sb are metallic, exhibiting specific resistivities at room temperature of the order of some mΩ cm, which decrease with decreasing temperature. The metallic character is also reflected in the calculated densities of states, which are shown for the structure model $Zr_5Ti_2Sb_7$ (*i.e.*, $Zr_{0.71}Ti_{0.29}Sb$) in the left part of Fig. 9 (calculated using the LMTO approach[27]). The lower part of the valence band is predominated by the Sb states, while metal and Sb states both contribute to the densities of states at the Fermi level E_F. The existence of Sb–Sb bonds reflects itself in the significant amount of unfilled Sb states (above E_F). The

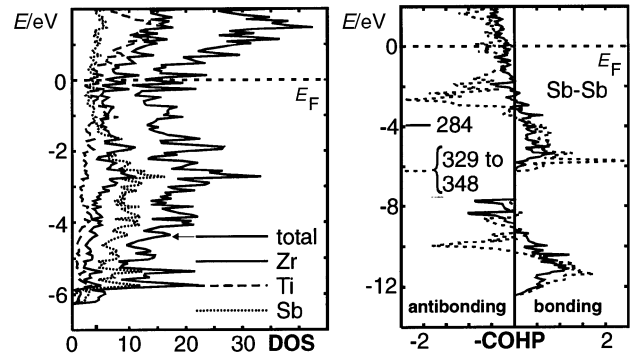

Fig. 9 DOS (left) and Sb–Sb COHP curves (right) of the structure model $Zr_5Ti_2Sb_7$.

Mulliken charges of the Sb atoms taking part in the Sb–Sb interactions of *ca*. 335 pm are averaged to be −0.31, comparable to the situation in $(Hf,Ti)_7Sb_4$ (−0.34), while the Sb atom with the short Sb–Sb bonds of 284 pm carries a Mulliken charge of −0.01 only. Comparable results were obtained for $(Zr,V)_{13}Sb_{10}$ and $(Zr,V)_{11}Sb_8$.[24]

The Sb–Sb interactions in the four antimonides $(Zr,V)_{13}Sb_{10}$, $(Zr,V)_{11}Sb_8$, $Ti_{11}Sb_8$, and (Zr,Ti)Sb can be divided into two different classes, namely those shorter than the shortest bond in the element (*i.e.* < 291 pm) and the one of the order of the longer bond length in the element (between 329 and 348 pm). The right part of Fig. 9 shows the crystal orbital Hamiltonian populations for the two different kinds for the case of the structure model $Zr_5Ti_2Sb_7$. As found for the two Sb–Sb contacts of 328 and 344 pm in $(Hf,Ti)_7Sb_4$, the longer interactions here exhibit almost as many filled antibonding as bonding states, whereas the filled bonding states outweigh the antibonding ones by far in the case of the short bond of 284 pm. The Mulliken populations of the longer ones are all small and positive (between 0.07 and 0.03), comparable to that in the element (335 pm, *MOP* = 0.08) and to those in $(Hf,Ti)_7Sb_4$ (0.05 and 0.02). Here again, the *MOP* values suggest bonding character of these interactions and thus the existence of unoccupied Sb states in all of these cases. This observation was expected, based on the perceptions gained in the case of the more metal-rich antimonide $(Hf,Ti)_7Sb_4$.

More striking is the occurrence of Sb–Sb distances in metal-rich antimonides, which are comparable to typical single bonds such as in KSb (d_{Sb-Sb}: 283–285 pm), *cyclo*-$Sb_5{}^{5-}$ (281–291 pm) and $Sb_{11}{}^{3-}$ (276–285 pm).[28] Also, since each Sb atom of the linear chains takes part in two of these bonds, one might expect Sb(−I) atoms forming zigzag chains as in KSb or as Te(0) in elemental tellurium. However, the linearity of the chains stands against single bonds, as Extended Hückel calculations of the structure model of an infinite Zr_7Sb_2 chain (positional parameter taken from $Zr_{7.5}V_{5.5}Sb_{10}$) revealed.[4] Both p_π and both p_π* bands of the two Sb atoms are filled, occurring well below the Zr centered states, while only one band (p_σ*) remains empty (Fig. 10). One can therefore consider these Sb atoms as Sb(−II), forming (delocalized) 1-electron-2-center *sigma* Sb–Sb bonds.

The formal bond order of ½ is reflected in the Mulliken overlap populations obtained from calculations of different structure models, namely $Zr_7V_6Sb_{10}$ [modeling $(Zr,V)_{13}Sb_{10}$], $Zr_8V_3Sb_8$ [modeling $(Zr,V)_{11}Sb_8$], and $Zr_5Ti_2Sb_7$ [modeling (Zr,Ti)Sb]. The *MOP* values are 0.45 and 0.26 in the first case (280–288 pm), 0.39 and 0.28 in the second (283–288 pm), and 0.38 in the last (284 pm). The average of these interactions (0.36) is slightly more than half of the 0.65 electrons per Sb–Sb single bond in KSb. A linear Sb chain was also found in the structure of La_3TiSb_5,[29] where the distance of 314 pm exhibits an overlap population of 0.26. Therein, the bond order can be taken from simple electron counting, which results in $(La^{3+})_3Ti^{4+}(Sb^{3-})_3(Sb^{2-})_2$ to be ½ in a Sb(−II) chain also. Using

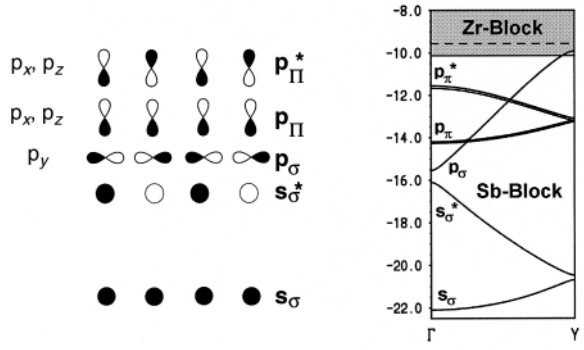

Fig. 10 Schematic band structure of a $_{\infty}{}^{1}[Zr_7Sb_2]$ chain.

Pauling's equation [$d(n) = d(1) - (60\ \text{pm} \times \log n)$], with n = bond order, r_{Sb} = 139 pm, the length of a Sb–Sb bond with a bond order of $\frac{1}{2}$ is calculated to be 296 pm.

The mismatches between bond length and bond strength in the cases of $(Zr,V)_{13}Sb_{10}$, $(Zr,V)_{11}Sb_8$, and (Zr,Ti)Sb are deduced to arise from matrix effects, namely from the equivalency of the *M*–*M* distances of the NiAs type fragments (r_{Ti} = 134 pm; r_V = 122 pm) and the Sb–Sb bonds and from the condensation *via* common faces of the $M^1{}_6Sb$ octahedra and $(M^1{}_7\square_1)Sb$ square antiprisms, respectively.

This mismatch is strongest in the case of the binary antimonide with the idealized composition $Ti_{11}Sb_8$ with b = 560 pm and $d_{Sb–Sb}$ = 276 and 284 pm. In that case, the steric stress is reduced by disorders in the Sb chain. According to the results of X-ray single crystal structure studies, the Sb site of this chain is never fully occupied. Additional neutron diffraction studies are underway for distinguishing between two models possible, *i.e.* an occupation of this site either with *ca*. 90% Sb and 10% vacancies or with *ca*. 80% Sb and 20% Ti.

However, the observed anomalies were motivation to subsequent attempts to substitute Sb in the linear chain in part by valence-electron-rich 3d metal atoms *M*′, since mixed *M*′/Sb occupancies were found in the antimonides $Hf_6M'_{1-x}Sb_{2+x}$,[30] $Zr_5M'_xSb_{3-x}$[1] and $Hf_{10}M'_xSb_{6-x}$ (*M*′ = V–Cu).[31] By incorporating the 3d metal atoms Mn, Fe, and Ni into the linear Sb chain of $Ti_{11}Sb_8$ up to 50%, corresponding to the idealized formula $Ti_{11}M'Sb_7$, the length of the *b* axis was decreased to 550 pm, because all *M*′ atoms used are smaller than the Ti and Sb atoms. In any case, no long range order was detected experimentally; however, the atoms within a given chain may be ordered, but then no ordering could occur from one chain to the next. The localized valence electrons of the Mn atoms in $Ti_{11}Mn_{0.52(1)}Sb_{7.48}$ cause Curie–Weiss behavior above 3 K, and antiferromagnetic ordering at lower temperatures, while the binary compound $Ti_{11}Sb_8$ exhibits the Pauli paramagnetism typical for metallic compounds (Fig. 11)

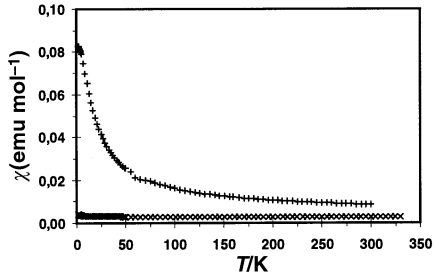

Fig. 11 Temperature dependencies of the magnetic susceptibilities of $Ti_{11}Sb_8$ (×) and $Ti_{11}Mn_{0.5}Sb_{7.5}$ (+) at 3 Tesla.

Comparable linear chains with mixed *M*′/Sb occupancies are exhibited in the structures of the isostructural antimonides $Hf_{10}M'_xSb_{6-x}$ and $Zr_5M'_xSb_{3-x}$. Both phases crystallize in a partially ordered variant of the W_5Si_3 type, which comprises parallel linear Si and W chains with short Si–Si and W–W bonds, respectively, of equivalent lengths. This type is basically limited to compounds of the groups 13 and 14, because the pnicogen and chalcogen atoms *E* are unlikely to form short *E*–*E* bonds in compounds with a *M*:*E* ratio of 5:3 = 1.67. Exceptions are the electron-precise compounds $(A^{2+})_{0.5}(K^{1+})_4(Te^{1-})(TeO^{2-})_2$ (with *A* = Ca and Sr), where not sufficient valence electrons of the *A* atoms are available to reduce all Te atoms to Te(−II). Therein, each Te(−I) atom forms two 1-electron-2-center bonds within the linear chains.[32] Furthermore, one binary vanadium arsenide crystallizes in the W_5Si_3 type, in the structure of which the As–As interactions are reduced by an incorporation of either vacancies or of vanadium in the chain.[1]

In the structures of the phases $Hf_{10}M'_xSb_{6-x}$, the Si site of the linear chain of the W_5Si_3 structure can be occupied by different *M*′/Sb mixtures varying between 3:1 and 2:3, with *M*′ being any 3d metal atom between V and Cu. The *M*′/Sb chain is located in face-condensed square antiprisms formed by Hf atoms (Hf2), running parallel to a chain of edge-condensed $Hf1Sb_4$ tetrahedra, whose Sb sites exhibit no *M*′ contribution (Fig. 12). The interatomic distances of the two different linear chains, formed by *M*′/Sb and Hf1, respectively, are about 280 pm, equal by symmetry.

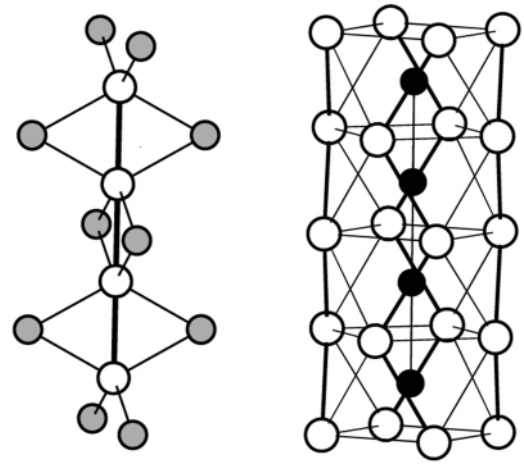

Fig. 12 Columnar structure motifs of $Hf_{10}M'_xSb_{6-x}$. White circles: Hf; black: *M*′/Sb; gray: Sb. Left: chain of $Hf1Sb_4$ tetrahedra. Right: chain of (*M*′,Sb)$Hf2_8$ square antiprisms.

By means of X-ray diffraction, no ordering of the *M*′ and Sb atoms was observed, independent of the preparation method. This is deduced to arise from a gain in the configurational entropy ΔS: $Hf_{10}M'_xSb_{6-x}$ cannot be obtained at reaction temperatures below 1350 °C, which corresponds to $T\Delta S$ = 0.2 eV at x = 1. This value is higher than the difference in the total energies of the structure models with and without ordering between the chains of 0.02 eV, as calculated with the LMTO approximation. With the free energy ΔG being determined by $\Delta G = \Delta H - T\Delta S$, complete ordering cannot be expected at the formation temperature of 1350 °C. No matter how the *M*′ and Sb atoms are located with respect to each other in the real structures, short Sb–Sb contacts of approximately 280 pm must occur if $x < 1$, a value which was reached experimentally.

Physical property measurements reveal the phases $Hf_{10}M'_xSb_{6-x}$ as metallic conductors, independent of the *M*′ atom used and independent of *x*. On the other hand, the magnetic properties do depend on *M*′: for x = 1, $Hf_{10}FeSb_5$ is the only example with ferromagnetic properties, while all other antimonides exhibit Pauli paramagnetism. These experimentally obtained observations are in agreement with the results of the LMTO calculations of the electronic structures.[31]

5 Sb layers in metal-rich antimonides

The binary vanadium antimonides of the valence-electron-poor transition elements with Sb layers cover the wide M:Sb range from 1.5 to 0.83. The structure of V_3Sb_2 exhibits planar Sb sheets consisting solely of hexagons, while the structure of ZrSb contains sheets of puckered Sb hexagons, reminiscent of the structure of the element. In both cases, however, the Sb–Sb distances are intermediate between the ones in the element of 291 and 335 pm, namely 320 pm in the case of V_3Sb_2 and 324 and 325 pm in ZrSb.[1] Correspondingly, the Mulliken overlap populations for these bonds are 0.17 in V_3Sb_2 and 0.06 and 0.09 in ZrSb.[13] Other planar sheets, consisting of Sb_4 squares, occur in the structures of $LnM'Sb_3$[26] and $LnM'Sb_2$.[33]

$V_{15}Sb_{18}$, $Ti_{8-x}Bi_9$ and $Hf_{8-x}Bi_9$ all form the same structure type, with $Zr_2V_6Sb_9$ occurring in an ordered variant thereof.[34] The structure of the latter (Fig. 13) consists in part of parallel to [001] running columns of face-condensed Zr-centered Sb_8 square antiprisms, chains of alternating Sb1 atoms and V_4 tetrahedra. The V_4 tetrahedra are connected *via* additional V atoms to form puckered layers perpendicular to [001].

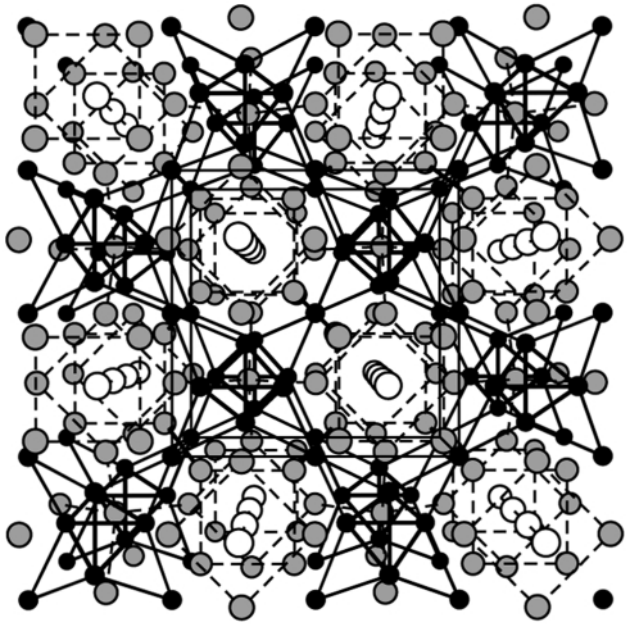

Fig. 13 Projection of the structure of $Zr_2V_6Sb_9$ along [001]. White circles: Zr; black: V; gray: Sb.

The $ZrSb_8$ square antiprisms contain two crystallographically distinct Sb_4 squares, both being ideal, exactly planar squares with interatomic distances of 337 (Sb2) and 343 pm (Sb3), respectively. The squares formed by Sb2 are interconnected *via* shorter Sb2–Sb2 bonds of 306 pm resulting in puckered semi-regular 48^2 nets, whereas the $Sb3_4$ squares are indirectly connected over Sb1 atoms *via* Sb1–Sb3 contacts of 336 pm. This results in planar squares and planar hexagons, interconnected to puckered layers (Fig. 14). Again, the bond lengths correlate well with the Mulliken overlap populations, which are 0.34 for the shortest bond (306 pm) and between 0.03 and 0.05 for the longer interactions (336–343 pm).

Aside from the occurrence of puckered Sb or Bi layers, the isostructural compounds $V_{15}Sb_{18}$, $Zr_2V_6Sb_9$ and Ti_8Bi_9 exhibit another striking feature, namely enlarged anisotropic displacement parameters (ADP) in the case of one metal site. That site is located in a E_8 square antiprism, with the M–E distances significantly longer (on average 14–17 pm per bond) than those of the second ME_8 antiprism, and with displacement parameters being larger by 50 to 100%. The high ADP values of the one M site can be understood as a consequence of the large M–E distances, pointing to a *rattling* of the M atom in a large E_8 cage.

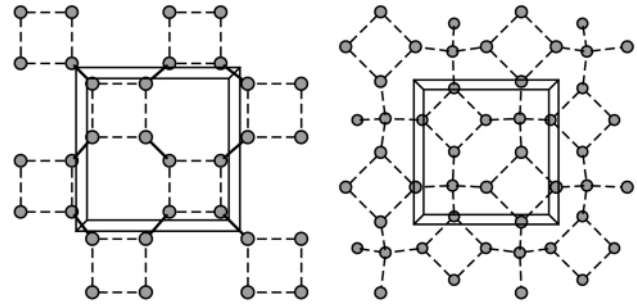

Fig. 14 Sb layers in the structure of $Zr_2V_6Sb_9$. Left: Sb2 layer; right: (Sb1,Sb3) layer.

Rattling usually results in a very low lattice contribution to the thermal conductivity, as observed for the filled skutterudites LnM'_4Sb_{12} (Ln = lanthanoids, M' = Fe, Co,…). Therein, the Ln atom is located in an Sb_{12} icosahedron, which leads to extraordinarily enhanced thermoelectric properties in the case of $LaFe_3CoSb_{12}$.[35] Thermoelectric properties are evaluated by the *figure-of-merit* Z or its dimensionless product $ZT = TS^2\sigma\kappa^{-1}$, with T = temperature, S = Seebeck coefficient, σ = electrical conductivity, and κ = thermal conductivity. The best materials are small-gap semiconductors (*i.e.* with a band gap of 0.1–0.3 eV) with high thermal stabilities exhibiting low thermal conductivities, which may arise from rattling atoms, mixed occupancies and low symmetry.[36] However, due to the metallic character of the M_8E_9 compounds discussed above, their overall thermoelectric properties are poor.

6 Three-dimensional Sb networks

The filled skutterudites mentioned above are examples of antimonides exhibiting three-dimensional Sb networks, consisting of Sb_4 squares with interatomic separations of roughly 290 pm, connected to a 3D network by longer Sb–Sb contacts of *ca.* 340 pm. Taking that as one possible fingerprint for good thermoelectrica, one needs to find antimonides with related networks, small band gaps and high thermal stabilities in order to get materials with outstanding thermoelectric properties. Metal-rich antimonides usually show the high thermal stabilities requested, but are rarely semiconductors. Hence, it is worthwhile to have a closer look at compounds with intermediate metal : antimony ratios, such as $(M',Ti)_5Sb_8$.[37] Note, however, that $(M',Ti)_5Sb_8$ does not conform to the criteria of metal-rich compounds with *e.g.* M' = Zr, since the 20 valence electrons of the metal atoms don't suffice to reduce the eight Sb atoms per formula unit to −III.

These phases can be obtained directly from the melt, *i.e.* by arc-melting in inert gas atmospheres, and exist with different M' atoms, namely at least Zr, Hf, Nb and Mo atoms. Single crystal structure studies reveal the phase range of $Zr_{5-x}Ti_xSb_8$ being within $1.1(3) \leqslant x \leqslant 3.9(1)$. The unprecedented crystal structure, presented in Fig. 15, contains three-dimensionally interconnected Sb as well as M atoms (M = M', Ti), the shorter Sb–Sb distances ranging from 316 to 337 pm, with M–M distances around 350–360 pm. All metal atom sites are mixed occupied by different M':Ti ratios, being surrounded by six to eight Sb atoms in the first coordination spheres.

The structural prerequisites for good thermoelectric properties are fulfilled in the case of $(M',Ti)_5Sb_8$. Physical property measurements, however, reveal these phases to be metallic (Fig. 16) with small Seebeck coefficients.

The results of the measurements are in agreement with the results of the LMTO calculation of the structure model Ti_5Sb_8, exhibiting the structural parameters taken from the structure refinements of $Zr_{1.1(1)}Ti_{3.9}Sb_8$. The valence band, consisting of both Ti and Sb states at the Fermi level, shows a pseudo gap *ca.* 1 eV above the Fermi level (left part of Fig. 17), which could be

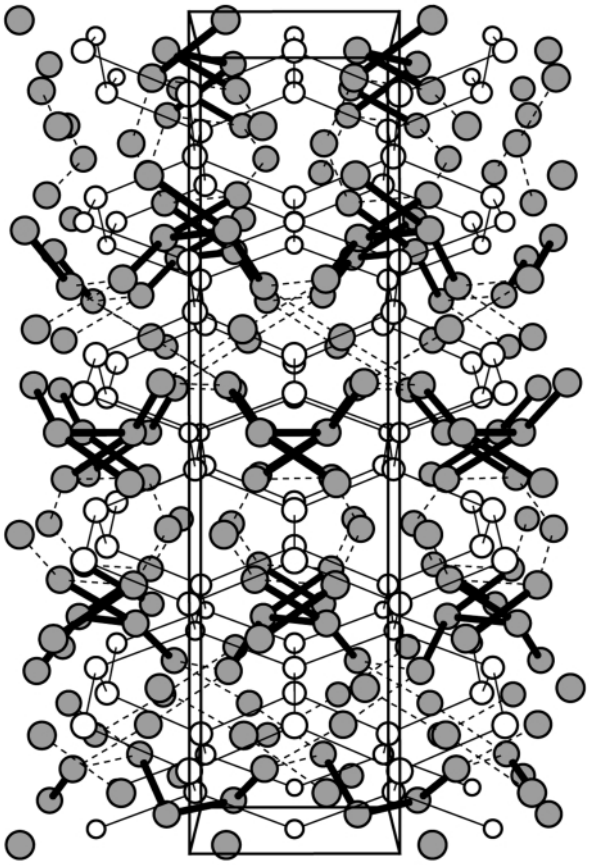

Fig. 15 Projection of the structure of $(M,Ti)_5Sb_8$ along [100]. White circles: *M*; gray: Sb.

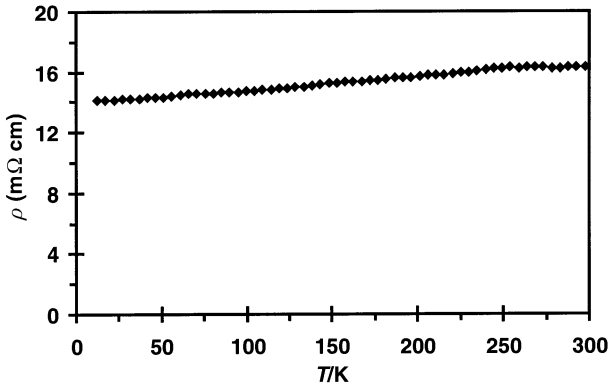

Fig. 16 Temperature dependence of the specific resistivity of $TiZr_4Sb_8$.

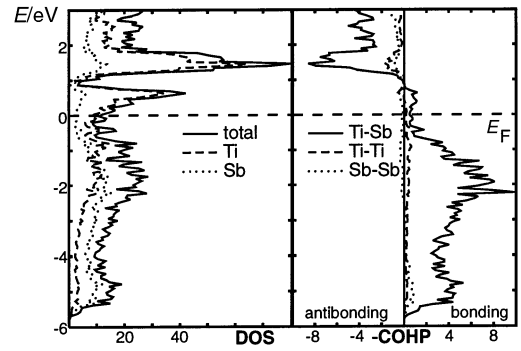

Fig. 17 DOS (left) and COHP curves (right) of the structure model Ti_5Sb_8.

reached by increasing the number of the valence electrons per formula unit by 10, *e.g.* by substituting in part *M'* by Mo and Sb by Te.

According to the calculated COHP curves, the structure is stabilized mainly by *M*–Sb bonds, and to a minor extent by *M*–*M* and Sb–Sb bonds (right part of Fig. 17). Increasing the number of valence electrons up to the pseudo gap would result in increased *M*–Sb and *M*–*M* bonding, but weaker Sb–Sb bonds because of the filling of more antibonding Sb–Sb states.

With respect to an efficient thermoelectric energy conversion, the synthesis of compounds crystallizing in the M_5Sb_8 type structure with 70 valence electrons per formula unit remains a challenging goal. In the same context, we are currently studying compounds based on Mo_3Sb_7 with 55 valence electrons which also exhibit a small band gap as well as an interesting Sb atom substructure.[38] Among the other Sb-rich antimonides of the valence-electron-poor transition elements like MSb_2 (*M* = Ti, Zr, Hf, V, Nb, Ta),[1] no band gaps are observed close to the corresponding Fermi levels, which is indicative of metallic properties of these compounds independent of the exact number of valence electrons. However, all of these structures are stabilized not only by the dominating heteronuclear *M*–Sb bonds, but also by both kinds of homonuclear interactions, namely *M*–*M* and Sb–Sb interactions. This is caused by the small electronegativity differences between the *M* and Sb atoms, which inhibit a complete oxidation of *M* by Sb.

7 Summary

The metal-rich antimonides reviewed in this article belong to those fascinating compounds, whose crystal structures exhibit homonuclear bonds between the cationic as well as the anionic constituent elements. Such structures were observed over the wide range of metal : antimony ratios between 1.75 and 0.625.

Table 1 Selected Sb atom substructures in transition metal antimonides

M : Sb	Formula	Sb units	d_{Sb-Sb}/pm	*MOP* (Sb–Sb)
1.75	$(Hf,Ti)_7Sb_4$	angled Sb_3 unit	328/344	0.05/0.02
1.5	V_3Sb_2	planar hexagonal sheets	320	0.17
ca. 1.4	$Ti_{11-x}Sb_{8-y}$	linear chains with defects	276/284	0.44/0.31
		zigzag chains	335–339	0.06–0.05
1.375	$(Zr,V)_{11}Sb_8$	linear chains	283/288	0.39/0.28
		zigzag chains	341–344	0.02
1.3	$(Zr,V)_{13}Sb_{10}$	linear chains	280/288	0.45/0.26
		zigzag chains	334–349	0.04–0.02
1	(Zr,Ti)Sb	linear double chains	284/348	0.38/0.06
		puckered 4^4 nets	329–344	0.07–0.03
1	ZrSb	puckered hexagonal sheets	324/325	0.06/0.09
0.888	$Zr_2V_6Sb_9$	puckered layers with pairs,	306	0.34
		squares, hexagons and octagons	336–343	0.05–0.03
0.625	$(Zr,Ti)_5Sb_8$	three-dimensional network	316–337	0.22–0.07

One can nicely follow the decreasing extent of reduction of the Sb atoms with decreasing M:Sb ratio, which occurs with increasing extensions of the Sb atom substructures, starting from Sb_3 units in $(Hf,Ti)_7Sb_4$, infinite Sb chains in $(Zr,V)_{13}Sb_{10}$, $(Zr,V)_{11}Sb_8$ and (Zr,Ti)Sb, and Sb layers in V_3Sb_2, ZrSb and $Zr_2V_6Sb_9$, and ending with the three-dimensional Sb atom substructures in $(M',Ti)_5Sb_8$, as summarized in Table 1.

The occurrence of both kinds of homonuclear interactions, namely *M–M* and *Sb–Sb* bonds, is associated with highly complex crystal structures, compared to those of the other pnictides and chalcogenides, because of the presence of three different types of bonding, *i.e.* the predominating heteronuclear bonds and the two different homonuclear interactions. In some cases, anomalies within the Sb atom substructure, *e.g.* in the linear Sb chains, rendered possible various (formal) substitution reactions, including substitution of Sb atoms by 3d metal atoms such as V, Cr, Mn, Fe, Co, Ni, Cu. These reactions led to different physical properties, the most striking of which being different cooperative magnetic phenomena.

The observed tendency of the Sb atoms to form extended complex networks might be used for the formation of new compounds exhibiting fairly low lattice thermal conductivities, and thus possibly enhanced thermoelectric properties as found in the filled skutterudites LnM'_4Sb_{12}.

8 References

1 P. Villars, *Pearson's Handbook, Desk Edition*; American Society for Metals: Materials Park, OH, 1997.
2 M. Conrad and B. Harbrecht, *J. Less-Common Met.*, 1992, **187**, 181.
3 P. A. Maggard and J. D. Corbett, *Angew. Chem., Int. Ed. Engl.*, 1997, **36**, 1974.
4 H. Kleinke, *Chem. Commun.*, 1998, 2219.
5 G. A. Marking and H. F. Franzen, *Chem. Mater.*, 1993, **5**, 678.
6 R. L. Abdon and T. Hughbanks, *Angew. Chem., Int. Ed. Engl.*, 1994, **33**, 2328.
7 X. Yao, G. J. Miller and H. F. Franzen, *J. Alloys Compd.*, 1992, **183**, 7.
8 M. Conrad, *PhD thesis*, Dortmund, Germany 1997; M. Conrad, F. Krumeich and B. Harbrecht, *Angew. Chem., Int. Ed.*, 1998, **37**, 1383.
9 H. Kleinke and H. F. Franzen, *Bol. Soc. Chil. Quím.*, 1997, **42**, 421.
10 H. Kleinke, K. M. Kleinke and H. F. Franzen, *J. Alloys Compd.*, 1996, **242**, 11; G. A. Marking and H. F. Franzen, *J. Am. Chem. Soc.*, 1993, **115**, 6126.
11 C.-C. Huang, J. Neuhausen and W. Tremel, *Chem. Commun.*, 2000, 17.
12 F. Hulliger, *Struct. Bonding*, 1968, **4**, 83.
13 H. Kleinke, unpublished calculations.
14 J. K. Burdett, *Chemical bonding in solids*, Oxford University Press, New York, 1995, and references cited therein.
15 R. Hoffmann, *J. Chem. Phys.*, 1963, **39**, 1397; M.-H. Whangbo and R. Hoffmann, *J. Am. Chem. Soc.*, 1978, **100**, 6093; R. S. Mulliken, *J. Chem. Phys.*, 1955, **23**, 2343. Program EHMACC, adapted for use on a PC by M. Köckerling, Gesamthochschule Duisburg, 1997.
16 K. W. Klinkhammer and P. Pykkö, *Inorg. Chem.*, 1995, **34**, 4134; H. Bürger, R. Eujen, G. Becker, O. Mundt, M. Westerhausen and C. Witthauer, *J. Mol. Struct.*, 1983, **98**, 265.
17 G. Papoian and R. Hoffmann, *J. Solid State Chem.*, 1998, **139**, 8.
18 B. Harbrecht and R. Leersch, *J. Alloys Compd.*, 1996, **238**, 13.
19 H. Kleinke and C. Felser, *J. Alloys Compd.*, 1999, **291**, 73.
20 H. Kleinke and B. Harbrecht, *Z. Anorg. Allg. Chem.*, 2000, **626**, 1851.
21 H. Kleinke, *Inorg. Chem.*, 1999, **38**, 2931.
22 H. Kleinke and H. F. Franzen, *J. Am. Chem. Soc.*, 1997, **119**, 12824, and references cited therein.
23 H. Kleinke, *J. Mater. Chem.*, 1999, **9**, 2703.
24 H. Kleinke, *Z. Kristallogr.*, 1999, Suppl. **16**, 42.
25 H. Kleinke, *J. Am. Chem. Soc.*, 2000, **122**, 853.
26 M. Brylak and W. Jeitschko, *Z. Naturforsch. B: Chem. Sci.*, 1995, **50**, 899; M. J. Ferguson, R. W. Hushagen and A. Mar, *J. Alloys Compd.*, 1997, **249**, 191.
27 O. K. Andersen, *Phys. Rev.*, 1975, **B12**, 3060; H. L. Skriver, *The LMTO Method*, Springer, Berlin, 1984; G. Krier, O. Jepsen, A. Burkhardt and O. K. Andersen, *The TB-LMTO-ASA program*, Version 4.7c; R. Dronskowski and P. Blöchl, *J. Phys. Chem.*, 1993, **97**, 8617.
28 N. Korber and F. Richter, *Angew. Chem., Int. Ed. Engl.*, 1997, **36**, 1512; U. Bolle and W. Tremel, *J. Chem. Soc., Chem. Commun.*, 1992, 91.
29 G. Bolloré, M. J. Ferguson, R. W. Hushagen and A. Mar, *Chem. Mater.*, 1995, **7**, 2229.
30 H. Kleinke, *J. Alloys Compd.*, 1998, **270**, 136.
31 H. Kleinke, C. Ruckert and C. Felser, *Eur. J. Inorg. Chem.*, 2000, 315.
32 I. Schewe-Miller and P. Böttcher, *J. Alloys Compd.*, 1992, **183**, 98.
33 O. Sologub, K. Hiebl, P. Rogl, H. Noël and O. Bodak, *J. Alloys Compd.*, 1994, **210**, 153; K. D. Myers, S. L. Bud'ko, I. R. Fisher, Z. Islam, H. Kleinke, A. H. Lacerda and P. C. Canfield, *J. Magn. Magn. Mater.*, 1999, **205**, 27.
34 S. Furuseth and H. Fjellvåg, *Acta Chem. Scand.*, 1995, **49**, 417; C. G. Richter and W. Jeitschko, *J. Solid State Chem.*, 1997, **134**, 26; H. Kleinke, *Eur. J. Inorg. Chem.*, 1999, 1369.
35 W. Jeitschko and D. J. Braun, *Acta Crystallogr.*, 1977, **B33**, 3401; D. T. Morelli and G. P. Meisner, *J. Appl. Phys.*, 1995, **77**, 3777; B. C. Sales, D. Mandrus and R. K. Williams, *Science*, 1996, **272**, 1325.
36 D. M. Rowe, *CRC Handbook of Thermoelectrics*, CRC Press, 1995; F. J. DiSalvo, *Science*, 1999, **285**, 703.
37 H. Kleinke, *New refractory antimonides—potentially thermoelectric materials*, in: Abstracts, 27th General Meeting of the GDCh, 1999; H. Kleinke, *Inorg. Chem.*, in press.
38 U. Häussermann, M. Elding-Pontén, C. Svensson and S. Lidin, *Chem. Eur. J.*, 1998, **4**, 1007.